JACS
JOURNAL OF THE AMERICAN CHEMICAL SOCIETY
Article
pubs.acs.org/JACS

High-Capacity Micrometer-Sized Li_2S Particles as Cathode Materials for Advanced Rechargeable Lithium-Ion Batteries

Yuan Yang,[†] Guangyuan Zheng,[‡] Sumohan Misra,[§] Johanna Nelson,[§] Michael F. Toney,[§,⊥] and Yi Cui*[,†,⊥]

[†]Departments of Materials Science and Engineering and [‡]Department of Chemical Engineering, Stanford University, Stanford, California 94305, United States

[§]Stanford Synchrotron Radiation Lightsource, SLAC National Accelerator Laboratory, Menlo Park, California 94025, United States

[⊥]Stanford Institute for Materials and Energy Sciences, SLAC National Accelerator Laboratory, 2575 Sand Hill Road, Menlo Park, California 94025, United States

Supporting Information

ABSTRACT: Li_2S is a high-capacity cathode material for lithium metal-free rechargeable batteries. It has a theoretical capacity of 1166 mAh/g, which is nearly 1 order of magnitude higher than traditional metal oxides/phosphates cathodes. However, Li_2S is usually considered to be electrochemically inactive due to its high electronic resistivity and low lithium-ion diffusivity. In this paper, we discover that a large potential barrier (~1 V) exists at the beginning of charging for Li_2S. By applying a higher voltage cutoff, this barrier can be overcome and Li_2S becomes active. Moreover, this barrier does not appear again in the following cycling. Subsequent cycling shows that the material behaves similar to common sulfur cathodes with high energy efficiency. The initial discharge capacity is greater than 800 mAh/g for even 10 μm Li_2S particles. Moreover, after 10 cycles, the capacity is stabilized around 500−550 mAh/g with a capacity decay rate of only ~0.25% per cycle. The origin of the initial barrier is found to be the phase nucleation of polysulfides, but the amplitude of barrier is mainly due to two factors: (a) charge transfer directly between Li_2S and electrolyte without polysulfide and (b) lithium-ion diffusion in Li_2S. These results demonstrate a simple and scalable approach to utilizing Li_2S as the cathode material for rechargeable lithium-ion batteries with high specific energy.

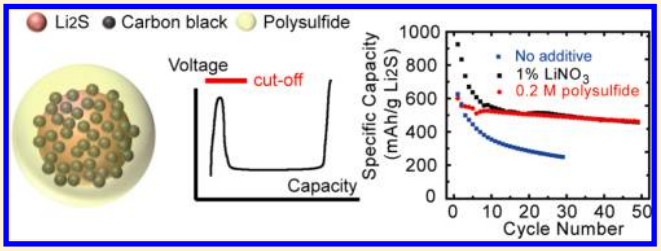

INTRODUCTION

Rechargeable lithium-ion batteries have been widely used in portable electronics and are promising for applications in electric vehicles and smart grids.[1−4] However, due to limited capacity in both electrodes, the specific energy of Li-ion batteries needs to be improved significantly to fulfill the requirements in these applications.[5,6] Significant improvement has been achieved in the development of high-capacity materials to replace carbon-based anodes, such as silicon[7−12] and tin.[13] However, state-of-the-art cathode materials have a capacity less than one-half of the carbon anode. Accordingly, breakthroughs in cathodes are urgently needed to increase the specific energy of lithium-ion batteries. Current metal oxide and phosphate cathodes possess an intrinsic capacity limit of ~300 mAh/g, with a potential of maximum 130% increase in the specific energy if all the capacity can be used.[14,15] In contrast, Li_2S has a specific capacity of 1166 mAh/g, four times that of the limit in oxide/phosphate cathodes.[15,16] Considering pairing with Si anodes with 2000 mAh/g capacity, the specific energy of a Li_2S-based lithium-ion battery could be 60% higher than the theoretical limit of metal oxide/phosphate counterparts (Figure 1A, see Supporting Information for details) and three times that of the current $LiCoO_2$/graphite system. Moreover, Li_2S could be paired with a lithium-free anode, preventing safety concerns and low Coulomb efficiency of lithium metal in Li/S batteries.[17,18]

The main hindrance for utilizing Li_2S is that it is both electronically and ionically insulating. Therefore, Li_2S was considered electrochemically inactive.[19] Recently, significant progress has been made to activate Li_2S. In our previous work, we reported a nanocomposite of Li_2S/mesoporous carbon with an initial capacity of 950 mAh/g. A full cell of Li_2S/silicon battery has also been demonstrated with a specific energy of 1000 Wh/kg based on the mass of active materials[15] (see Supporting Information for details). A ball-milled micrometer-sized Li_2S electrode with polymer electrolyte was reported to reach capacity close to the theoretical limit but with a large hysteresis (~1.6 V) and low energy efficiency (<50%) for the full cell.[20] Discharge capacities around 300 mAh/g were also observed in carbon/Li_2S composite electrodes at room temperature.[21,22] A Li_2S/indium cell with solid state electrolyte was also demonstrated recently with promising performance.[23] In this work, we show that there is a potential barrier of ~1 V at

Received: May 30, 2012
Published: August 21, 2012

   dx.doi.org/10.1021/ja3052206 | J. Am. Chem. Soc. 2012, 134, 15387−15394

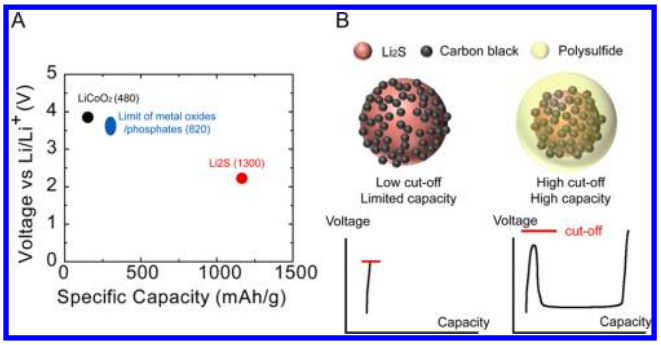

Figure 1. (A) Comparison of different cathode materials for lithium-ion batteries. Numbers in parentheses are the specific energy of a battery made of the cathode and a silicon anode with a specific capacity of 2000 mAh/g and potential of 0.45 V vs Li/Li^+. Li_2S/silicon battery could provide specific energy 60% higher than the theoretical limit of current metal oxide/phosphate cathodes. Only the mass of active materials is considered. (B) Schematic diagram illustrating the effect of applying a high cutoff to activate Li_2S. After overcoming the initial barrier, a polysulfide phase is formed and Li_2S becomes active.

the beginning of the first charging of Li_2S. By simply applying a higher voltage cutoff to overcome this barrier, Li_2S can be oxidized to polysulfides and rendered active (Figure 1B). After this activation process, the barrier does not appear again in subsequent cycling. An initial discharge capacity higher than 800 mAh/g is observed. Moreover, stable cycling has been achieved. The discharge capacity at the 10th cycle reaches 523 mAh/g based on the mass of Li_2S, and after that the capacity decays only ~0.25% per cycle. This method represents a simple and scalable approach to activate Li_2S, which has not been discovered before. In addition, as the size of Li_2S particles was in the micrometer range, the tap density of the electrode can be largely enhanced compared to their nanostructured counterpart.[15]

EXPERIMENTAL SECTION

Li_2S particles were purchased from Alfa Aesar. Sample without further modification is denoted as "pristine". Ball-milled Li_2S particles were prepared by mixing pristine Li_2S and Al_2O_3 (Sigma Aldrich) with a weight ratio of 95:5 and ball milled for 6 h (SPEX 8000D miller). Lithium nitrate was also purchased from Sigma Aldrich. Polysulfide solution was prepared by stirring pristine Li_2S and sulfur in 1,3-dioxolane overnight at 60 °C. The as-synthesized solution has a nominal molecular formula of Li_2S_8, and the concentration of sulfur is 0.2 M. To form electrodes for electrochemical testing, Li_2S particles, Super P carbon black, and polyvinylidene fluoride (Kynar) were ground together at a weight ratio of 40:45:15 in a mortar for 10 min and then stirred in *N*-methyl-2-pyrrolidone (NMP) for 12 h so that the content of Li_2S in pristine and ball-milled samples is 40% and 38% in weight, respectively. Next, the slurry was drop cast onto carbon paper (AvCarb P50T) and heated at 110 °C for 1 h inside a glovebox. The mass loading of the electrode is 1−1.5 mg Li_2S/cm^2. 2032-type coin cells (MTI Corp.) were used for two-electrode testing with lithium metal as the counter electrode. Cyclic voltammetry and impedance measurements were performed under a three-electrode configuration in pouch cells. A small piece of lithium was used as reference electrode and placed between Li_2S and lithium electrodes. All electrodes are separated by polymer separators. Electrolyte is 1.0 M lithium bis(trifluoromethanesulfonyl)imide (LiTFSI, Sigma Aldrich) in 1,3-dioxolane and 1,2-dimethoxyethane (v:v = 1:1). Electrode preparation and cell assembly were done in a glovebox with O_2 and H_2O less than 2 and 0.1 ppm, respectively. All C rates are based on the theoretical capacity of Li_2S (1C = 1166 mA/g). The frequency range for the impedance measurement is from 200 kHz to 0.01 Hz. In-situ synchrotron diffraction was performed at Stanford Synchrotron Radiation Lightsource beamline 11-3 with an X-ray energy of 12.74 keV. Experimental details were described in our previous work.[24] COMSOL 3.4 was used for simulation.

RESULTS AND DISCUSSION

Figure 2 illustrates the morphology of both pristine and ball-milled Li_2S particles. The typical particle size of pristine Li_2S is

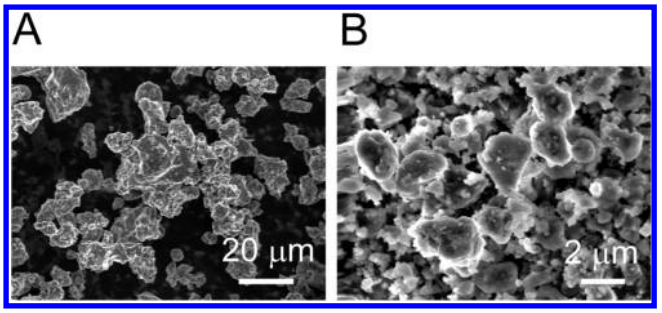

Figure 2. SEM images of (A) pristine Li_2S particles and (B) ball-milled Li_2S particles. Pristine samples have an average diameter of ~10 μm, while the size of the ball-milled one is ~2 μm.

~10 μm. Large particles with diameters up to 20 μm were also frequently observed in the pristine sample. After ball milling, the particle size decreases to 1−3 μm with an average size of 2 μm.

The voltage profile in the initial three cycles for pristine Li_2S at C/20 (58.3 mA/g) is presented in Figure 3a. A large barrier was apparent up at the beginning of the first charging. The voltage reached 3.45 V vs Li/Li^+ at a charging capacity of 48 mAh/g and then drops. The barrier was followed by a long flat plateau at ~2.4 V, suggesting a two-phase reaction. Afterward, the voltage jumps up and extra capacity was also extracted above 3.5 V, which was likely due to the imperfect mixing or poor contact between some Li_2S particles and carbon additives. The total capacity extracted in the initial charging was 982 mAh/g. In the first discharge, the typical two-plateau behavior of sulfur cathode was observed[25,26] and a discharge capacity of 804 mAh/g has been achieved, which is ~70% of the theoretical limit. The large charging barrier disappeared in the following cycles, and the voltage profile became similar to common sulfur electrodes.[26,27] This results in a low hysteresis (~0.2 V) between charge and discharge and thus high energy efficiency (85−90%), which is a dramatic improvement compared to previous results on Li_2S.[20]

The charging barriers were observed in both pristine and ball-milled samples at different rates (Figure 3B and 3C). Barrier heights were in the range of 0.9−1.5 V, which were calculated as the difference between maximum voltage in the barrier and the plateau voltage. The plateau voltage is generally 2.4−2.5 V in the range of C/20−C/8. After overcoming the barrier, significant capacity could be discharged in both types of samples. For example, an initial discharge capacity of 835 mAh/g was achieved at C/20 for ball-milled Li_2S electrodes, and the capacity at C/8 was maintained at 696 and 626 mAh/g for ball-milled and pristine Li_2S electrodes, respectively. It should be noted that the theoretical capacity of Li_2S with the mass of lithium counted is 70% of sulfur. To compare our results with sulfur cathode, which is currently being intensively studied, the capacity based on the mass of sulfur in Li_2S is also plotted on the top axis (Figure 3B and 3C). This activation behavior was also observed in our Li_2S/mesoporous carbon nanocomposite

dx.doi.org/10.1021/ja3052206 | J. Am. Chem. Soc. 2012, 134, 15387−15394

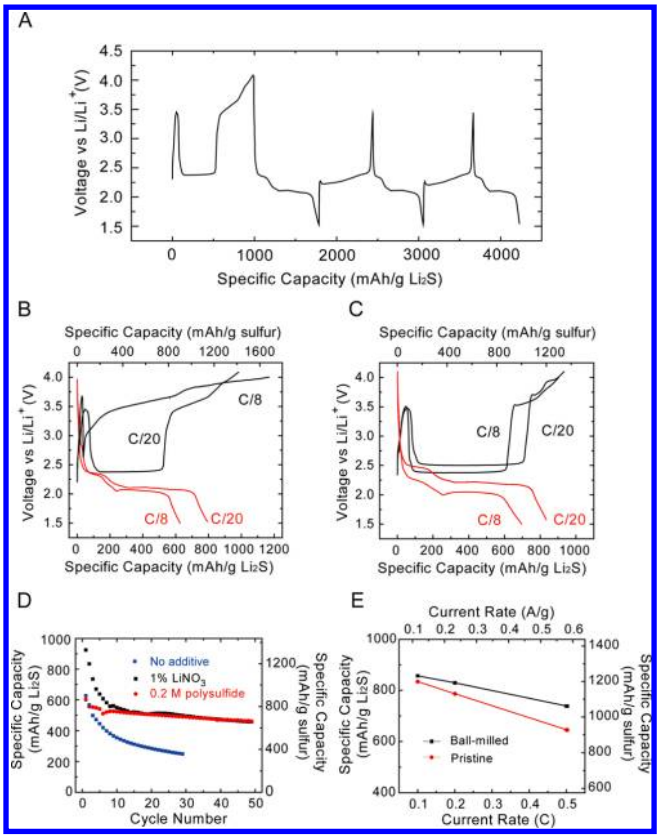

Figure 3. Electrochemical characteristics of micrometer-sized Li_2S electrodes. (A) Voltage profile of a pristine Li_2S electrode in the initial three cycles. As-made cell is in the discharged state, and it is charged first. Potential barrier was observed only at the beginning of the first charge. Electrode was charged to 4.1 V vs Li/Li^+ first and then cycled between 1.5 and 3.5 V. (B and C) Voltage profile of pristine (B) and ball-milled (C) Li_2S in the first cycle at C/20 and C/8. Voltage window is 1.5−4.1 V for C/20 and 1.5−4.0 V for C/8. Electrolyte used in A−C was 1.0 M LiTFSI in DOL/DME without additive. Top axes in both B and C are based on the mass of sulfur in Li_2S. (D) Cycling performance of pristine Li_2S particles without additive (blue), with 1% $LiNO_3$ (black), and with 0.2 M polysulfide (red). All electrodes were charged to 3.8 V at C/25 first and then cycled between 3.5 and 1.5 V at a current rate of C/10. (E) Rate capability of pristine and ball-milled Li_2S electrode with 1% $LiNO_3$ additive in the electrolyte. Capacities in the second discharge were plotted. Capacity remains over 700 mAh/g at 0.5 C (583 mA/g) for the ball-milled sample. Right axes in both D and E are based on the mass of sulfur in the Li_2S.

but with a much smaller amplitude (0.18 V), as the characteristic dimension of Li_2S in the composite was only about 3−10 nm.[15] In general, this barrier is universal in Li_2S samples. Statistically we found that a smaller current rate leads to a lower barrier, which will be discussed later in this paper. Initial activation was also confirmed by cyclic voltammetry measurements, which are shown in Figure S1, Supporting Information. In the initial sweep, anodic peaks were observed at 3.65 and 3.45 V vs Li/Li^+ for pristine and ball-milled samples, respectively. Peak positions do not indicate that oxidation of Li_2S occurs at such high potentials but that a high overpotential is necessary to overcome the initial barrier and render Li_2S electrochemically active. Redox peaks in the following cycles occur at positions of common sulfur cathodes, indicating that the cathode behaves in the same way as common sulfur electrodes.[28]

The cycling performance of pristine Li_2S electrodes is illustrated in Figure 3D. All samples were charged at C/25 to 3.8 V first and then cycled at C/10 between 1.5 and 3.5 V vs Li/Li^+. Without any additive, the Li_2S electrode showed a fast decay, similar to common sulfur cathodes.[27,29−31] However, the cycling performance was improved dramatically by introducing additives into the electrolyte. For example, with 1% $LiNO_3$ in the electrolyte, the initial discharge capacity reached 950 mAh/g at C/10. The discharge capacity was stabilized at 540 mAh/g at the 11th cycle, and the capacity of 460 mAh/g remained at the 50th cycle, corresponding to capacity retention of 85% in 40 cycles. Adding polysulfide into the electrolyte can also help improve the cycle life. When 20 μL Li_2S_8 solution ([S] = 0.2 M) was added into the electrolyte, the discharge capacity at the 10th and 50th cycles were 523 and 461 mAh/g, respectively, leading to a capacity decay of only 0.3% per cycle. The cycling performance of cells with polysulfide additive was further tested up to 100 cycles. The capacity decay rate was only 0.22% per cycle between the 10th and the 100th cycles (Figure S2, Supporting Information). The total amount of sulfur in the polysulfide additive was ∼10% of that in the Li_2S electrode, so the majority of the capacity originates from Li_2S. The improvement is likely a result of minimized material loss on the surface of lithium. $LiNO_3$ is well known to passivate the surface of lithium metal and significantly improve the Coulomb efficiency.[29,32,33] Polysulfide additives can compensate for material loss due to side reaction on the surface of lithium. The fact that Li_2S shrinks in the initial charge instead of expansion for sulfur cathodes may also contribute to the improved capacity retention, as it has less damage to the electrode integrity. The Coulomb efficiency was 95−97% for samples with $LiNO_3$ additives and 75−80% for those with polysulfide in the electrolyte. The Coulomb efficiency for Li_2S electrode without any additive was 80−90%. Similar cycling performance was also observed in ball-milled Li_2S, suggesting that particle size has little effect on the cycle life of Li_2S in the range of 1−10 μm, as Li_2S is converted to polysulfides after the initial charge in both pristine and ball-milled samples.

Good capacity retention at high rates was also observed in the Li_2S electrodes (Figure 3E). For pristine samples, the capacity remained at 645 mAh/g at 0.5 C (583 mA/g), which was 77% of that at 0.1 C. In the ball-milled samples, the capacity even reached 738 mAh/g at 0.5 C, 86% of that at 0.1 C. In all rate capability tests, 1% $LiNO_3$ was added to the electrolyte to reduce the impedance at the lithium/electrolyte interface and prevent material loss due to side reaction on the surface of metallic lithium. It should be noticed that 5−10% of discharge capacity in the second cycle arises from the $LiNO_3$ additive.

Results above show that Li_2S is a promising candidate as a high-capacity cathode for Li-ion batteries. Along with studies on Li_2S, a high-energy Li/S battery is currently an active field and plenty of progress has been achieved in improving its performance.[5,14,25,34−36] Thus, it is meaningful to compare the characteristics of these two systems. The theoretical specific energy of the Li/S system is 2600 Wh/kg, 70% higher than the Li_2S/silicon system (1550 Wh/kg).[15] However, practically, significantly more lithium is required in Li/S batteries due to formation of mossy lithium and the low Coulomb efficiency of lithium.[16] Consequently, the practical specific energy of Li_2S/silicon (930 Wh/kg) is close to that of the Li/S battery (1000 Wh/kg) (see Supporting Information for detailed calculations). The Li_2S/silicon system also avoids the safety issue in Li/S

dx.doi.org/10.1021/ja3052206 | J. Am. Chem. Soc. 2012, 134, 15387−15394

batteries. One possible issue of the Li_2S cathode is its reaction with moisture to generate toxic H_2S so that a dry room or glovebox is necessary for electrode fabrication and assembly. Full cell tests are also critical for evaluating practical applications of Li_2S.

As described above, by applying a high voltage cutoff in the initial charging, we demonstrated a simple and scalable method for activating Li_2S, especially given the fact that this material is air sensitive. No extra processing, such as lithiation or high-temperature processing to form carbon/Li_2S composite, is needed. Moreover, our approach is also compatible with conventional liquid electrolyte and room temperature operation. To our knowledge, this activation behavior is novel and has not been observed in other battery systems. It is thus meaningful to elucidate the mechanism behind the phenomenon in order to guide further improvement of this material. There are two basic questions to answer: (1) What is the reaction mechanism, such as the charging product and whether it is a single-phase or two-phase reaction and (2) what is the origin of the large initial potential barrier?

To answer these questions, in-situ synchrotron diffraction was used first to study the phase evolution in the initial charge. Diffraction patterns at different stages of charging are plotted in Figure 4. Numbers on the right side represent the amount of

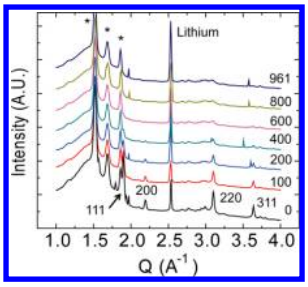

Figure 4. In-situ X-ray diffraction patterns of Li_2S electrode during the initial charging. Li_2S peaks were indicated with the indexing and disappeared on charging, but no extra peaks belonging to sulfur were detected. Numbers on the right represent the charging capacity. Asterisks (*) correspond to peaks from the plastic bag and the polymer separator.

capacity extracted. All Li_2S peak intensities decreased monotonously, showing that Li_2S is oxidized during charging. Meanwhile, no extra peaks corresponding to sulfur were observed so that crystalline sulfur was not formed. Several sharp peaks were observed at random stages of the charging. They are likely to come from other components in the cell, such as the plastic bag and separators, since they were also observed in other tests even without Li_2S electrodes. We also notice that the electrolyte turned yellow during the charging process, which is clear evidence that the charging product in the plateau region is soluble lithium polysufides.

The long flat plateau in the charge (Figure 3 A–C) and the initial barrier are both characteristics of the two-phase reaction. The origin of the barrier could be explained by phase nucleation where an extra driving force is needed to nucleate the new phase (polysulfides in this system), as observed in other materials with a two-phase reaction before, such as $LiFePO_4$.[37] This is further confirmed by the experiment of intentionally adding polysulfide solution into the electrolyte. The initial barrier disappeared after adding polysulfide solution into the electrolyte, as polysulfide nuclei already existed and thus extra free energy for phase nucleation was not required (Figure S3, Supporting Information). These results demonstrate that the reaction in the plateau region in the initial charge is a two-phase reaction between Li_2S and polysulfides, and the origin of the initial barrier is phase nucleation. However, the barrier height may be not solely determined by phase nucleation. Other kinetic processes, such as ionic transport, electronic conductivity, and charge transfer, also accompany the phase nucleation process in the initial barrier. These kinetic factors could contribute significantly to the amplitude of the potential barrier, especially at high current rates. As a result, it is important to determine the dominant factor for this large barrier to obtain a complete understanding of the electrochemical process and guide further improvement of Li_2S.

We first examine the contribution of the thermodynamic component, which is approached at the low current limit where effects of kinetic factors are negligible. Figure 5A shows the

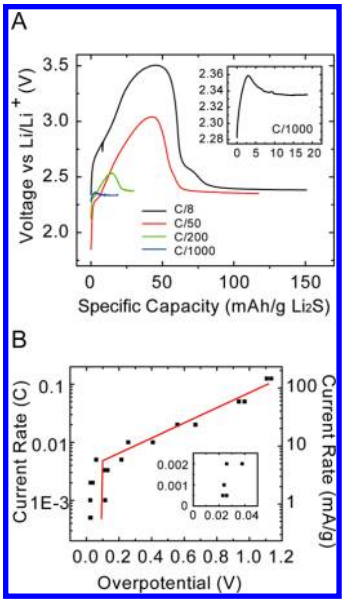

Figure 5. Relation between current rates and overpotentials. (A) Initial potential barrier at C/8, C/50, C/200, and C/1000. 1C = 1166 mA/g. (Inset) Zoom-in image of the barrier at C/1000. (B) Relation between the current rate and the overpotential. There are two regions. At rates higher than C/200, the overpotential depends linearly on the logarithm of the current. At rates lower than C/300, the overpotential is approximately constant. (Inset) Low rate region (<C/300). Red line is for eye guiding. Units in both insets are the same as the figures.

profiles of voltage barriers in a large current range from C/8 to C/1000 for the ball-milled sample. Barrier height strongly depends on the current rate, for example, 1.15 V at C/8 and only 25 mV at C/2000. Overpotentials at different current rates are plotted in Figure 5B. The relation can be divided into two regions, as guided by the red line. At higher current (>C/200), there is a linear relation between the overpotential and logarithm of the current rate. In contrast, the overpotential is nearly constant and quite small at low current (C/2000–C/500), which is the energy needed for phase nucleation since this approaches the zero-current limit and thus thermodynamics dominates.[38] The inset in Figure 5B shows the low-current region. The overpotential approaches ~20 mV at zero current. This small overpotential is negligible compared to the large barrier height (0.5–1 V) at moderate rates (C/50–C/8). As a result, kinetic factors are believed to dominate the height of the

dx.doi.org/10.1021/ja3052206 | J. Am. Chem. Soc. 2012, 134, 15387–15394

barrier when current is higher than C/100, reasonable rates for practical applications. This does not conflict with the previous statement that the initial barrier originates from phase nucleation of polysulfides. In our measurements, the contributions of all kinetic factors to the barrier height are concomitant with the phase nucleation process. At extremely low current rate (≤C/500) where kinetic factors have little effect on the electrochemical process, observation of the initial barrier indicates its thermodynamic origin from phase nucleation. As the current rate increases, the overpotential associated with kinetic factors also increases exponentially and finally dominates the height of the total barrier at high current (>C/100), as shown in Figure 5B. Similar behavior was also observed in pristine Li_2S samples, which were larger than the ball-milled ones. However, the thermodynamic limit was not reached even at current as low as C/5000 (0.23 mA/g) for pristine Li_2S (Figure S4, Supporting Information). In order to keep the whole analysis consistent, ball-milled Li_2S particles were used as the model system for the following mechanism studies, although pristine Li_2S samples showed the same trend.

Three kinetic factors might be responsible for the large barrier height: electronic conductivity of Li_2S, diffusivity of lithium ions in Li_2S, and charge transfer process at the surface of Li_2S particles. Other factors, such as ionic transport in the electrolyte, should contribute little to the overpotential as the current density is low (~200 $\mu A/cm^2$ for C/8). The solid electrolyte interphase on the lithium surface is also negligible since a large overpotential was not observed after the initial barrier. To understand the effect of these factors, we focus on the point when Li_2S cathode was charged to the top of the potential barrier, where the largest overpotential was reached.

The contribution of electronic conductivity was studied first as Li_2S is an electronically insulating material. The effect of electronic conductivity is measured as the immediate voltage drop when current is turned off at the top of the barrier, since electronic transport is a fast process.[39] Measurements have been done in both the coin cell and the pouch cell configuration, and similar results were observed. The initial voltage drop is as small as less than 10 mV at both C/20 and C/200 (Figure S5, Supporting Information). One concern in this measurement is that electrons may not respond as fast as that in common battery materials due to the high resistivity of Li_2S. To address this issue, the charge relaxation time t was estimated.[40] The calculated relaxation time is less than ~0.2 s, and thus, the effect of electronic transport is negligible after 1 s. The corresponding voltage drop at 1 s is also negligible (<30 mV) compared to the large potential barrier (Figure S5, Supporting Information). Consequently, the effect of electronic conductivity is negligible, and the barrier is dominated by either ionic transport inside Li_2S or the charge transfer process on the surface of Li_2S particles. Details of analyses are presented in the Supporting Information.

To understand the effect of lithium-ion diffusivity and charge transfer, a suitable model is needed to describe the electrochemical process in the barrier region. We followed the work by the Newman group, where the Butler–Volmer model was used as the governing equation.[41,42] At the top of the potential barrier, the polysulfide phase is not yet formed. Consequently, the electrochemical reaction is still within the single-phase regime

$$Li_2S(s) \rightarrow Li_{2-x}S(s) + xLi^+ + xe^- \qquad (*)$$

The extracted lithium ions migrate into the electrolyte and electrons move to the current collector through the carbon additives, leaving deficient $Li_{2-x}S$ in the solid state. As a result, the reaction only happens at the boundary of the three phases: Li_2S, carbon additives, and electrolyte. The relation between overpotential (η) and current rate (j) can be described as

$$j = j_0(C_S/C_T)^{\alpha}(\exp((1-\alpha)F\eta/RT) - \exp(-\alpha F\eta/RT)) \qquad (1)$$

where j_0 is the exchange current, C_S is the concentration of lithium ions on the surface, and C_T is the concentration of lithium ions in stoichiometric Li_2S. α is the transfer coefficient, F is the Faraday constant, R is the ideal gas constant, and T is the temperature. At the top of the barrier, the overpotential η is a large positive value so that the second exponential term is negligible and the expression can be simplified to

$$j = j_0(C_S/C_T)^{\alpha}\exp((1-\alpha)F\eta/RT) \qquad (2)$$

This expression illustrates that overpotential should be proportional to the logarithm of the current, which is consistent with our results (Figure 5B), suggesting that the process is dominated by charge transfer. It also shows that the overpotential only relates to ionic transport inside Li_2S through C_S, the surface concentration of ions. The overpotential due to ionic transport then can be calculated as the difference between two cases: the real situation and the case that diffusivity is so high that it does not contribute to the overpotential.[43] Consequently, the overpotential due to ionic transport is expressed as

$$\eta_{ion} = \frac{\alpha RT}{(1-\alpha)F}\ln\frac{C'}{C_S}, \qquad (3)$$

C' is the concentration of lithium ions at the surface of the Li_2S particle at the top of the potential barrier when diffusivity is very high (see "The Effect of Ionic Transport" part in the Supporting Information for details). The lithium-ion concentration on the surface of Li_2S is very difficult to measure experimentally. Instead, simulation was used to obtain the surface concentration of lithium ions in different cases. The Nernst–Planck equation was used to describe the process, and the movement of lithium ions and electrons was treated as a binary electrolyte.[44] We found that the surface concentration of lithium ions decreased as the current increased, since a larger concentration gradient is needed at higher current rate to maintain the continuous current at the Li_2S/electrolyte interface. For example, the concentration of Li^+ is ~35% of that in stoichiometric Li_2S at C/20, while it is 85–90% at C/200 (Figure S7, Supporting Information). As a result, the Li_2S particle has a core/shell-like structure when charged to the top of the barrier. The shell is highly lithium deficient Li_2S, and the core is nearly stoichiometric Li_2S, as described in Figure S7, Supporting Information. Simulation details are presented in the Supporting Information.

By applying the simulated surface concentration of lithium ions and experimental overpotential, current data in eq 2, parameters such as α and j_0 could be determined. α is fitted to be 0.91 ± 0.01, and j_0 is $3 \pm 1 \times 10^{-7}$ A/cm^2 with a correlation coefficient of 0.99. The high correlation coefficient suggests that the model adequately described the electrochemical process. α of 0.91 is a very large transfer coefficient as common values for α are between 0.3 and 0.7.[45] The high α means that the applied overpotential is very ineffective in adjusting the

dx.doi.org/10.1021/ja3052206 | J. Am. Chem. Soc. 2012, 134, 15387–15394

energy barrier for oxidation of Li_2S. Substituting $\alpha = 0.91$ into eq 3, overpotentials due to ionic transport (η_{ion}) were calculated, as shown in Figure 6A. In the range of C/20−C/200, η_{ion} accounts for about 15−30% of the total overpotential, indicating that it contributes to the barrier to a certain extent, especially at high rates. However, it is not the dominant factor for the high potential barrier. The sensitivity of results to C_S is estimated by changes of fitting parameters (e.g., α and j_0) upon variation in diffusivities and mobilities. It is found that changes in C_S do not affect the conclusion that ionic transport is not the dominant factor, as the charge transfer term in the Butler−Volmer model is an exponent function while the diffusion term is only a power function and the power α is less than 1. For example, if both the diffusivity and mobility are doubled, though C_S changes by about 50%, α only lowers to 0.90 and j_0 is not affected. Consequently, η_{ion} decreases to only 60 mV as the ionic transport is faster. Detailed discussions are shown in "the effect of ionic transport-discussion" section in the Supporting Information. We would like to emphasize that the purpose of analyses above is to understand the mechanism behind the large barrier but not identify the contribution of each factor quantitatively.

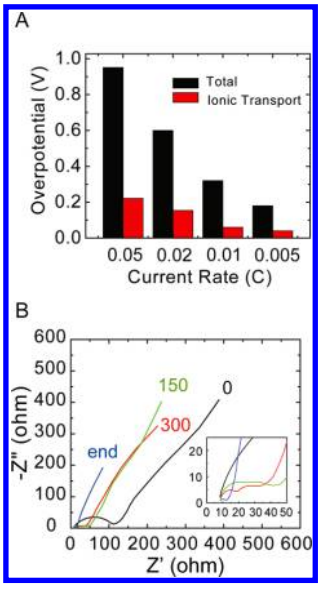

Figure 6. (A) Contribution of ionic transport to the total overpotential at different rates. Limitations in ionic transport account for 15−30% of the total overpotential. (B) Evolution of impedance during the charging process. Numbers in the figure indicate the amount of capacity extracted. Diameter of semicircles shrinks when more capacity was extracted from the Li_2S electrode, indicating better charge transfer upon charging. Two semicircles in the middle of charging suggest a two-step charge transfer process. The number in (B) is the charged capacity in the unit of mAh/g. Frequency range is from 200 kHz to 0.01 Hz. (Inset) Zoom-in image of the impedance results. Units are the same as the large figure.

The remaining overpotential is considered to arise from the charge transfer process. This is consistent with a small j_0 of $3 \pm 1 \times 10^{-7}$A/cm^2 based on the model above. This value is several orders of magnitude smaller than traditional cathodes, such as $LiCoO_2$[46] and $LiFePO_4$,[47] indicating that this process is difficult for Li_2S. The charge transfer process could be described as follows. In the single-phase reaction regime (Li_2S (s) → $Li_{2-x}S$ (s) + $xLi^+ + xe^-$) from the beginning of charge to the top of barrier lithium ions and electrons at the surface of Li_2S are extracted from solid Li_2S particle and move to the electrolyte and conductive carbon black, respectively, leaving deficient solid $Li_{2-x}S$ with the same crystal structure as Li_2S. The low exchange current and high transfer coefficient are likely due to the fact that Li_2S is an ionic crystal, and the strong bonding between Li^+ and S^{2-} ions makes it very difficult to extract Li^+ from Li_2S to the electrolyte when no polysulfide exists in the electrolyte, and thus, the bonding environment for Li^+ changes drastically from Li_2S to the electrolyte. Regarding the contribution of electrons and ions to the charge transfer process, as they are both involved in the process (reaction marked with an asterisk (*)), it is hard to separate them and answer which one dominates, but we believe that the overall charge transfer process controls the overpotential and is the main reason for the large potential barrier.

Our model also explains other experimental observations, which further corroborate its validity. It is consistent with the evolution of impedance results in the initial charge (Figure 6B). Before charging, only a single semicircle was observed for the

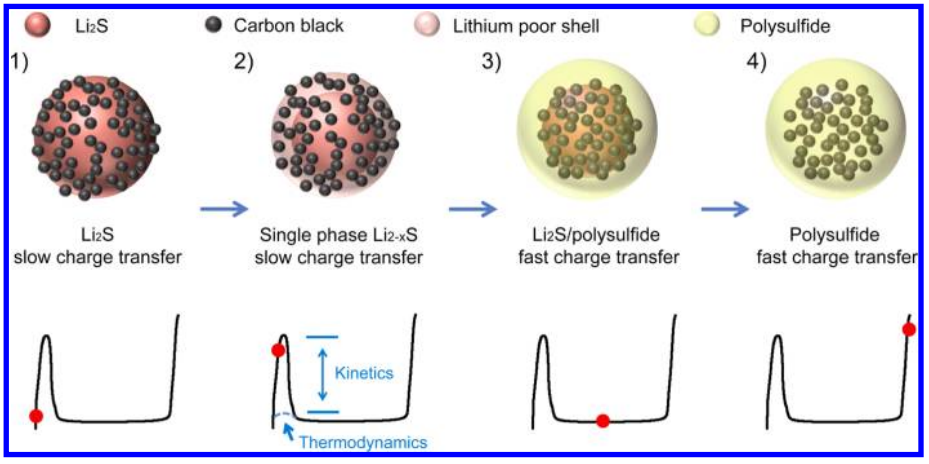

Figure 7. Summary of the model for the initial charging of Li_2S. Before reaching the top of the potential barrier, $Li_{2-x}S$ exists as a single phase with a lithium-poor shell on the surface. In step 2, the shell is highly lithium deficient while the core remains in near stoichiometry. In step 3, soluble polysulfides are formed after overcoming the initial barrier, shown as the yellow part around the solid Li_2S particle. Consequently, the kinetics is significantly improved. At the end of charging, only the polysulfide phase exists with a fast kinetics.

dx.doi.org/10.1021/ja3052206 | J. Am. Chem. Soc. 2012, 134, 15387−15394

charge transfer process, and the corresponding charge transfer resistance (R_{ct}) is ~120 ohms. In the middle of charging, for example, after 150 and 300 mAh/g capacity were extracted, two semicircles with smaller R_{ct} of 10−20 ohms were observed. However, at the end of charging, only one semicircle remains with an even smaller R_{ct} of ~3 ohms. Such evolution could be explained as the electrochemical reaction varies along with the charging (Figure 7)

before the barrier top (steps 1 and 2):

$$Li_2S(s) \rightarrow Li_{2-x}S(s) + xLi^+ + xe^-$$

in the middle of charging (step 3):

$$yLi_2S(s) \rightarrow Li_2S_y(l) + (2y - 2)Li^+ + (2y - 2)e^-$$

$$Li_2S_y(l) \rightarrow y/8Li_2S_8(l) + (2 - y/4)Li^+ + (2 - y/4)e^-$$

at the end of charging (step 4):

$$Li_2S_y(l) \rightarrow y/8Li_2S_8(l) + (2 - y/4)Li^+ + (2 - y/4)e^-$$

The first charge transfer process is slow according to analyses above, leading to a large charge transfer resistance (Figure 7, steps 1 and 2). The core/shell-like structure in step 2 indicates that the surface layer of Li_2S is highly lithium deficient due to the low ionic diffusivity of lithium ion in Li_2S, but both the core and the shell remain in a single solid phase. In the middle of charging, two steps occur: from Li_2S to polysulfides in the electrolyte (yellow), and redox reaction between soluble polysulfide species. As the lithium bonding environment in Li_2S is more like that in polysulfides than in pure electrolyte, it is reasonable to assume that the charge transfer process is easier between Li_2S and the polysulfide. The second step should be quite fast as species involved are in the liquid phase. Consequently, two semicircles with much smaller diameter (10−20 ohms) were observed in the middle of charging (Figure 7, step 3). At the end of charging, only the polysulfide phase exists, and thus, only one semicircle remains (Figure 7, step 4). The assumption of faster kinetics between Li_2S and polysulfide is validated by the impedance of Li_2S electrode in the electrolyte with polysulfide additives (Figure S8, Supporting Information). Even before charging, two semicircles show up in the impedance as polysulfide acts as an intermediate species for charge transfer. Moreover, the diameters of the two semicircles are only 30−50 ohms, much smaller than that without polysulfide additives, which further confirms that the charge transfer between Li_2S and polysulfide is easier.

The model above also answers why there is little overpotential after the initial activation in the first charge. First, as discussed above, the charge transfer process was significantly improved after formation of polysulfide nuclei in the electrolyte. Second, since polysulfide nuclei occur in the electrolyte after activation, any small deficiency in lithium ions at the surface of Li_2S particles will lead to immediate phase separation, and thus, $\ln(C'/C_S)$ is close to 0. Consequently, the overpotential due to ionic transport (η_{ion}) is also negligible and a plateau with little overpotential was observed after initial activation in the first charge.

In summary, we demonstrate a simple and scalable approach to activate micrometer-sized Li_2S particles. By applying a high charging cutoff voltage to overcome the initial potential barrier, polysulfide phase is formed, which dramatically improves the kinetics of Li_2S, such as the charge transfer process. This novel approach can turn even 10 μm-sized Li_2S electrochemically active and leads to a discharge capacity as high as 850 mAh/g. With either polysulfide or $LiNO_3$ additives in the electrolyte, the cycle retention was improved to 85−88% from the 11th to the 50th cycles with a specific capacity of 500−550 mAh/g. The decay rate is only 0.22% per cycle between the 10th and the 100th cycles for the sample with polysulfide additive. The mechanism behind this novel phenomenon is also studied. The origin of the initial barrier is phase nucleation, but the height of the barrier is mainly a result of poor charge transfer at the surface of Li_2S and limited diffusivity of lithium ions inside Li_2S. The results reported here provide a practical approach to utilize Li_2S as cathode material for lithium-ion batteries. It could potentially lead to rechargeable batteries with specific energy four times that of the state-of-the-art technology.

■ ASSOCIATED CONTENT

Ⓢ Supporting Information

Descriptions of more experiments and simulations. This material is available free of charge via the Internet at http://pubs.acs.org.

■ AUTHOR INFORMATION

Corresponding Author

E-mail: yicui@stanford.edu

Notes

The authors declare no competing financial interest.

■ ACKNOWLEDGMENTS

A portion of this work was supported by the Department of Energy, Office of Basic Energy Sciences, Division of Materials Sciences and Engineering under contract DE-AC02-76SF0051 through the SLAC National Accelerator Laboratory, Laboratory Directed Research and Development funding, under contract DE-AC02-76SF00515 (J.N., M.F.T., Y.C.). Y.C. acknowledges support from a King Abdullah University of Science and Technology (KAUST) Investigator Award (No. KUS-l1-001-12). Y.Y. acknowledges financial support from the Stanford Graduate Fellowship (SGF). G.Z. acknowledges financial support from the Agency for Science, Technology and Research (A*STAR), Singapore. Portions of this research were carried out at the Stanford Synchrotron Radiation Lightsource, a national user facility operated by Stanford University on behalf of the U.S. Department of Energy, Office of Basic Energy Sciences.

■ REFERENCES

(1) Tarascon, J. M.; Armand, M. *Nature* **2001**, *414*, 359−367.
(2) Whittingham, M. S. *Chem. Rev.* **2004**, *104*, 4271−4301.
(3) Kang, B.; Ceder, G. *Nature* **2009**, *458*, 190−193.
(4) Chung, S. Y.; Bloking, J. T.; Chiang, Y. M. *Nat. Mater.* **2002**, *1*, 123−128.
(5) Ji, X. L.; Nazar, L. F. *J. Mater. Chem.* **2010**, *20*, 9821−9826.
(6) Goodenough, J. B.; Kim, Y. *Chem. Mater.* **2010**, *22*, 587−603.
(7) Chan, C. K.; Peng, H. L.; Liu, G.; McIlwrath, K.; Zhang, X. F.; Huggins, R. A.; Cui, Y. *Nat. Nanotechnol.* **2008**, *3*, 31−35.
(8) Zhou, S.; Liu, X.; Wang, D. *Nano Lett.* **2010**, *10*, 860−863.
(9) Wu, H.; Chan, G.; Choi, J. W.; Ryu, I.; Yao, Y.; McDowell, M. T.; Lee, S. W.; Jackson, A.; Yang, Y.; Hu, L.; Cui, Y. *Nat. Nanotechnol.* **2012**, *7*, 1−6.
(10) Liu, N.; Wu, H.; McDowell, M. T.; Yao, Y.; Wang, C.; Cui, Y. *Nano Lett.* **2012**, *12*, 3315−21.
(11) Cui, L. F.; Yang, Y.; Hsu, C. M.; Cui, Y. *Nano Lett.* **2009**, *9*, 3370−3374.

(12) Cui, L. F.; Ruffo, R.; Chan, C. K.; Peng, H. L.; Cui, Y. *Nano Lett.* **2009**, *9*, 491−495.
(13) Derrien, G.; Hassoun, J.; Panero, S.; Scrosati, B. *Adv. Mater.* **2007**, *19*, 2336−2340.
(14) Ji, X. L.; Lee, K. T.; Nazar, L. F. *Nat. Mater.* **2009**, *8*, 500−506.
(15) Yang, Y.; McDowell, M. T.; Jackson, A.; Cha, J. J.; Hong, S. S.; Cui, Y. *Nano Lett.* **2010**, *10*, 1486−1491.
(16) Bruce, P. G.; Freunberger, S. A.; Hardwick, L. J.; Tarascon, J.-M. *Nat. Mater.* **2012**, *11*, 19−30.
(17) Brissot, C.; Rosso, M.; Chazalviel, J. N.; Lascaud, S. *J. Power Sources* **1999**, *81*, 925−929.
(18) Liu, X. H.; Zhong, L.; Zhang, L. Q.; Kushima, A.; Mao, S. X.; Li, J.; Ye, Z. Z.; Sullivan, J. P.; Huang, J. Y. *Appl. Phys. Lett.* **2011**, *98*, 183107.
(19) Obrovac, M. N.; Dahn, J. R. *Electrochem. Solid State Lett.* **2002**, *5*, A70−A73.
(20) Hassoun, J.; Scrosati, B. *Angew. Chem., Int. Ed.* **2010**, *49*, 2371−2374.
(21) Takeuchi, T.; Sakaebe, H.; Kageyama, H.; Senoh, H.; Sakai, T.; Tatsumi, K. *J. Power Sources* **2010**, *195*, 2928−2934.
(22) Kim, J.; Hassoun, J.; Panero, S.; Sun, Y.-K.; Scrosati, B. *Green* **2011**, *1*, 323−328.
(23) Nagao, M.; Hayashi, A.; Tatsumisago, M. *J. Mater. Chem.* **2012**, *22*, 10015−10020.
(24) Nelson, J.; Misra, S.; Yang, Y.; Jackson, A.; Liu, Y.; Wang, H.; Dai, H.; Andrews, J. C.; Cui, Y.; Toney, M. F. *J. Am. Chem. Soc.* **2012**, *134*, 6337−6343.
(25) Jayaprakash, N.; Shen, J.; Moganty, S. S.; Corona, A.; Archer, L. A. *Angew. Chem., Int. Ed.* **2011**, *50*, 5904−5908.
(26) Liang, C. D.; Dudney, N. J.; Howe, J. Y. *Chem. Mater.* **2009**, *21*, 4724−4730.
(27) Wang, H.; Yang, Y.; Liang, Y.; Robinson, J. T.; Li, Y.; Jackson, A.; Cui, Y.; Dai, H. *Nano Lett.* **2011**, *11*, 2644−2647.
(28) Yang, Y.; Yu, G. H.; Cha, J. J.; Wu, H.; Vosgueritchian, M.; Yao, Y.; Bao, Z. N.; Cui, Y. *ACS Nano* **2011**, *5*, 9187−9193.
(29) Barchasz, C.; Leprêtre, J.-C.; Alloin, F.; Patoux, S. *J. Power Sources* **2011**, *199*, 322−330.
(30) Choi, Y. J.; Chung, Y. D.; Baek, C. Y.; Kim, K. W.; Ahn, H. J.; Ahn, J. H. *J. Power Sources* **2008**, *184*, 548−552.
(31) Yuan, L. X.; Yuan, H. P.; Qiu, X. P.; Chen, L. Q.; Zhu, W. T. *J. Power Sources* **2009**, *189*, 1141−1146.
(32) Zheng, G.; Yang, Y.; Cha, J. J.; Hong, S. S.; Cui, Y. *Nano Lett.* **2011**, *11*, 4462−4467.
(33) Aurbach, D.; Pollak, E.; Elazari, R.; Salitra, G.; Kelley, C. S.; Affinito, J. *J. Electrochem. Soc.* **2009**, *156*, A694.
(34) Ji, X.; Evers, S.; Black, R.; Nazar, L. F. *Nat. Commun.* **2011**, *2*, 325.
(35) Zheng, G. Y.; Yang, Y.; Cha, J. J.; S, S. S.; Cui, Y. *Nano Lett.* **2011**, *11*, 4462−4467.
(36) Xiao, L.; Cao, Y.; Xiao, J.; Schwenzer, B.; Engelhard, M. H.; Saraf, L. V.; Nie, Z.; Exarhos, G. J.; Liu, J. *Adv. Mater.* **2012**, *24*, 1176−1181.
(37) Wagemaker, M.; Mulder, F. M.; Van der Ven, A. *Adv. Mater.* **2009**, *21*, 2703−2709.
(38) Meethong, N.; Huang, H.-Y. S.; Speakman, S. a.; Carter, W. C.; Chiang, Y.-M. *Adv. Funct. Mater.* **2007**, *17*, 1115−1123.
(39) Hu, L. B.; Choi, J. W.; Yang, Y.; Jeong, S.; La Mantia, F.; Cui, L. F.; Cui, Y. *Proc. Natl. Acad. Sci. U.S.A.* **2009**, *106*, 21490−21494.
(40) Sze, S. M.; Ng, K. K. *Physics of Semiconductor Devices*; Wiley, J., Ed.; Wiley: New York, 2007; Vol. *9*.
(41) Doyle, M.; Newman, J.; Gozdz, A. S.; Schmutz, C. N.; Tarascon, J.-M. *J. Electrochem. Soc.* **1996**, *143*, 1890−1903.
(42) Doyle, M.; Fuller, T. F.; Newman, J. *J. Electrochem. Soc.* **1993**, *140*, 1526−1533.
(43) Srinivasan, V.; Newman, J. *J. Electrochem. Soc.* **2004**, *151*, A1517−A1529.
(44) Newman, J.; E. Thomas-Alyea, K. *Electrochemical Systems*, 3rd ed.; John Wiley & Sons: New York, 2004.
(45) Bard, A. J.; Faulkner, L. R. *Electrochemical Methods Fundamentals and Applications*; John Wiley & Sons: New York, 2001.
(46) Zhao, J.; Wang, L.; He, X.; Wan, C.; Jiang, C. *Int. J. Electrochem. Sci.* **2010**, *5*, 478−488.
(47) Zhang, Y.; Feng, H.; Wu, X.; Wang, L.; Zhang, A.; Xia, T.; Dong, H.; Liu, M. *Electrochim. Acta* **2009**, *54*, 3206−3210.